



Optimization strategy for flexible barrier structures: Investigation and back analysis of a rockfall disaster case in southwestern China

Li-Ru Luo¹, Zhi-Xiang Yu^{1,2}, Qi Wang³, Li-Jun Zhang¹, Lin-Xu Liao¹, Li Peng⁴,

¹ Department of Civil Engineering, Southwest Jiaotong University, Chengdu, 610036, China

² National Engineering Research Center of Geological Disaster Prevention in Land Transportation, Chengdu, 611730, China

³ Southwest Electric POWER Design Institute Co., Ltd. of China Power Engineering Consulting Group, Chengdu, 610051, China

⁴ Sichuan OST Slope Protection Engineering Co., Ltd., Chengdu, 610011, China

10 *Correspondence to:* Zhi-Xiang Yu (yzxzrq@swjtu.edu.cn)

Abstract. Field investigations and back analyses were conducted on a rockfall hazard. The flexible barrier protection system constructed along the roadside got damaged by the rockfall impact and lost its ability to mitigate. Vital physical characteristics like rockfall trajectory and kinetic energy were presumed based on the data from an aerial survey and the slope digital model. A numerical model, including slope, rockfalls, and flexible barrier, was created, so the impacting process was reproduced. It demonstrates that the rockfall's impact kinetic energy is only around 40% of its design protection energy. The improper connections of members are the leading causes of damage, which prevent the flexible barrier from producing significant deformation and reduce its capacity to absorb impact force. The damage can be avoided by changing the members' connections to improve the nets' and ropes' ability to slide and deform. The calculation results indicate that the optimized model's performance in terms of complete protection is three times better than the actual project's. The findings can be used as a guide when designing a flexible protection system that performs better.

1 Introduction

Flexible protection system has been widely employed in transportation, land, minerals, and energy, among others, to prevent and control geological disasters on slopes. The flexible barrier, one of the flexible protection system's structural variations (Volkwein et al., 2011; Gentilini et al., 2012; Shi, 2013; Luo et al., 2022), is particularly well-known for its effectiveness as a defense against high-energy impact hazards like falling rocks, debris flows, mudslides, and avalanches (Peila and Ronco, 2009; Rorem et al., 2013; Kwan et al., 2014). The flexible barrier is a structural system made up of the supporting part, the intercepting part, the connecting part, the energy dissipation part, and the anchoring part. It protects by absorbing the kinetic energy of impact from the disaster through the system's significant inelastic deformation (Yu et al., 2018a; Volkwein et al., 2019a; Ferrero et al., 2015; Jiang et al., 2020). Some products have passed the 10,000kJ impact test (Geobruigg, 2017). In actual engineering, however, the flexible barrier is frequently damaged even if the impact energy is lower than the design protection energy. It cannot provide the desired level of protection. The primary cause of this appearance is the disparity



between the idealized test conditions and the variety of actual engineering conditions, such as impact effects, system installation forms, and component connection relationships, which results in the mitigation measure's decreased reliability in practical applications. To fully utilize the protective capabilities of flexible barriers, it is crucial to comprehend how these aspects affect them.

Most current research focuses on the mechanical behavior and damage mechanisms of flexible nets and anchors in controlled laboratory settings (Spadari et al., 2012; Wang et al., 2013). Since of the complexity, only little study has been done on the failure and damage mechanisms of the flexible barrier in actual engineering environments. Margreth and Roth (2008) investigated and found that the anchor ropes and steel column bases were the most susceptible components of the flexible barrier applied for avalanche protection. According to Kwan et al.'s (2014) analysis of a flexible barrier damaged by debris flow impact, the protective structure's faulty connection caused the support posts to buckle, and they suggested an optimization strategy. In response to the rockfall impact, some scholars investigated 15 flexible barrier projects damaged by the rockfall. These studies clarified that the flexible rockfall barrier primarily experienced five types of damage, including support post instability, post foot damage, steel wire rope breakage, anchor pullout, and component corrosion (Zhao et al., 2016; Lei and Luo, 2021; Yu et al., 2019b; Liu, 2020). Among them, (Yu et al., 2019b) and (Zhao et al., 2016) particularly studied the mechanisms and optimized countermeasures for support post instability and steel wire rope breakage. In actual projects, the impact damage effect of rockfall on the flexible barrier is highly random, so it is difficult to fully consider these damage effects in the forward design method commonly used. Therefore, it is necessary to conduct a back analysis to thoroughly research the damage mechanism and performance improvement countermeasures for flexible barrier projects. It is of great significance to improve the reliability of mitigation measures design.

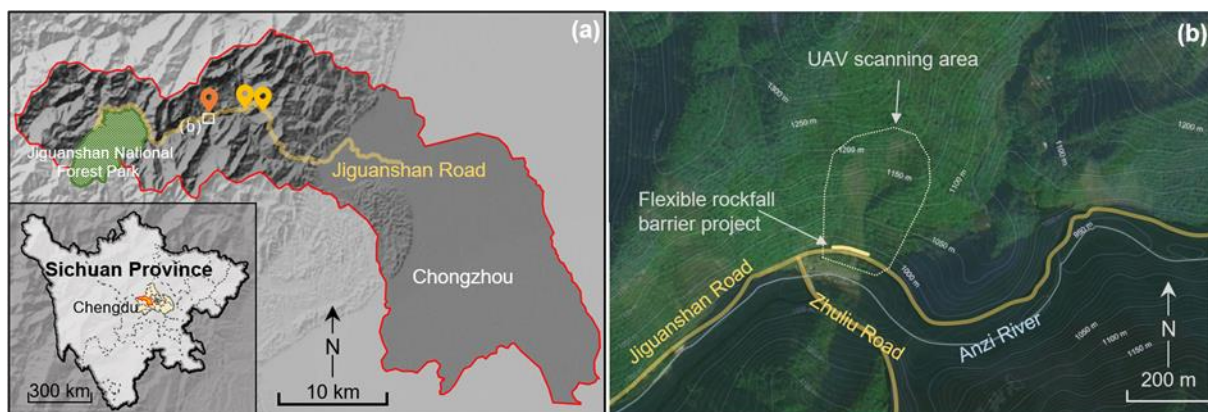
A flexible rockfall barrier was damaged by a rockfalls impact on the road leading to the Jiguanshan National Forest Park in Chengdu, Sichuan Province, China. The damage characteristics of the flexible rockfall barrier were investigated. At the same time, a digital slope model was created based on a UAV aerial survey, and essential physical characteristics, including the rockfall trajectory and impact kinetic energy, were assumed. Combining the investigation information, a FEM model containing a part of the slope, the rockfalls, and the flexible rockfall barrier was established. A back analysis of the dynamic process of rockfalls impacting the protection system was then performed to replicate the damage evolution process of the protection system and to reveal the damage mechanism of the actual protection project. Finally, optimized design strategies were proposed with the same material types and specifications used in the existing project. Compared with the inverse model, the optimized model avoids the damage phenomenon found by the investigation and improves the protection capability by at least three times. The research results of this paper can provide a reference for improving the reliability of flexible rockfall barrier design.

2 Field investigation

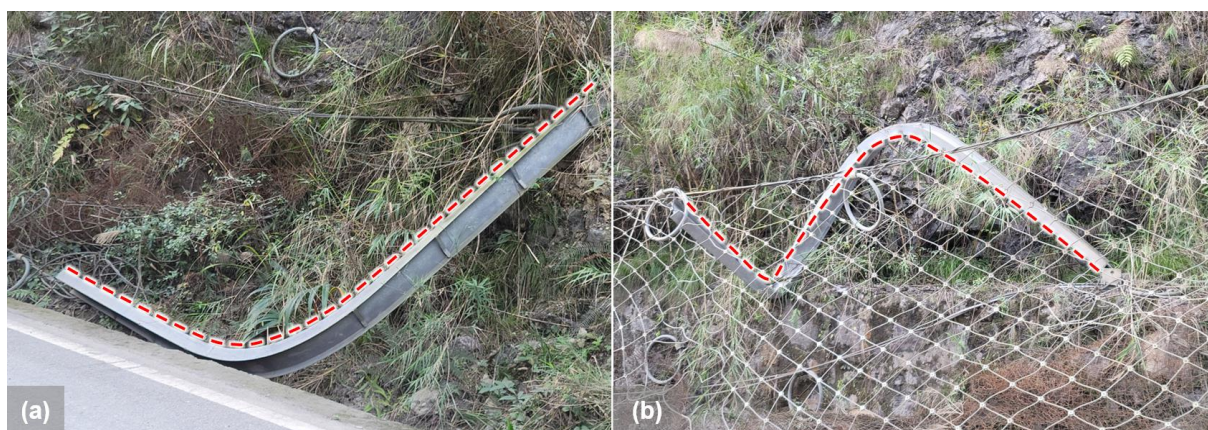
2.1. Description of the study site in Jiguanshan



As shown in Fig. 1a, Jiguanshan National Forest Park is situated in Chongzhou, southwest of Chengdu, with its back toward
65 Longmen Mountain and its front facing the Chengdu Plain, and in the middle south section of the Longmen Mountain structural
belt, with complex structural conditions. The southeast of Chongzhou is plain, the center and western regions the southeast are
hilly, and the broad western areas are covered with low mountain high mountain landforms. The faults and folds in the low
mountain regions of the west cause the rock mass to be broken, cause the cleavage ssure to develop, deeply cut the terrain, and
70 result in a significant relative height difference (Yang et al., 2023). The authors investigated multiple cave-in rockfall disasters
that damaged the flexible barriers along the Jiguanshan Road leading to the Jiguanshan National Forest Park in mid-November
2020. Three flexible rockfall barrier projects with similar structural forms experienced system overturning and damage from
buckling steel columns, with the most common buckling forms being "C"-shaped compression buckling and "S"-shaped
bending and torsion buckling (Fig. 2). This paper provides a detailed investigation and analysis of a disaster site where rockfalls
had not been cleared at that time (Fig. 1b).



75
Figure 1: Geological map of the rockfall disasters: (a) Regional terrain and the location of the three disaster sites. Map data: <https://mywis.cn/> and ©Aliyun 2022; (b) Regional aerial image of the case focused in this paper. Image: www.tianditu.gov.cn.



80
Figure 2: Steel column buckling forms of the other two flexible rockfall barrier projects: (a) "C"-shaped compression buckling and
(b) "S"-shaped bending and torsion buckling.



Drone aerial photography and measuring tools make up most of the survey methods. The DJI Mavic 2pro drone, whose precision is 2000 pixels, was used to capture aerial photography. Tape measure, vernier caliper, and a standard scale with 1-millimeter and 0.1-millimeter precision were used for measuring.

Based on the slope inclination photography information obtained by the UAV, a 3D digital model of the terrain was constructed with the help of ContextCapture software (Bentley, 2021), with a reduction accuracy of centimeter level. The 3D model of the scanned slope is depicted in Fig. 3a; it is roughly 276 meters high and slopes at a 45° angle, with a steep top and a gentle bottom. The hill was primarily covered by medium-high shrubs and bushes. Its foot was predominantly covered by plants like ferns, bamboo, and reed-like herbs, typical in southern and southwestern China. Sedimentary rock formations were exposed in the concave cavity area in the middle of the slope, and numerous hazardous rocks were created by the prolonged penetrating joints and fissures that divided the rock into broken blocks or pieces of various sizes. The area on the slope where new rock layers were exposed after rock spalling was presumed to be the source of rockfalls. The rockfall source was located 105 meters above the stopping point at the bottom of the hill and was 22 meters lateral along the road. A small amount of gravel and debris was scattered in the gully, and the vegetation along the front section of the gully was severely destroyed. About 2 meters wide, the gully had a minor quantity of rubble and garbage spread throughout it, and the vegetation along the front half of the gully had been severely devastated (Fig. 3). Rockfalls had been stopped by the retaining walls and the flexible rockfall barrier built at the foot of the slope.

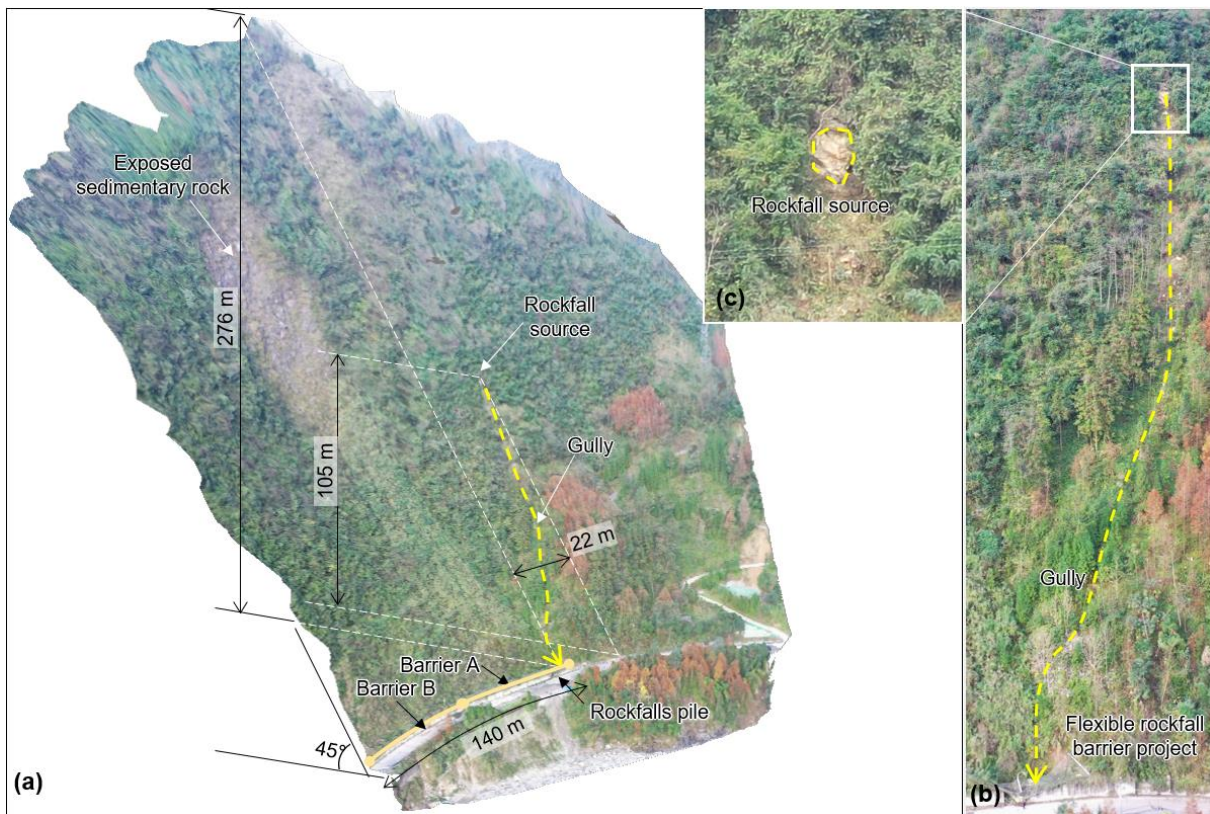




Figure 3: Investigation results of the rockfall source area and trajectory. (a) The digital model of the slope; (b) Rockfall impact gully; (c) Rockfall source.

100 Many intercepted rockfalls, mostly tuff and muddy, were pocketed inside the nets of the protection system, as depicted in Fig. 4, with sharp angles and disparate blocks. The four largest blocks of these stones could be approximated as four cubes: Stone 1 was $0.5\text{m} \times 0.5\text{m} \times 0.5\text{m}$, Stone 2 was $0.3\text{m} \times 0.3\text{m} \times 0.7\text{m}$, Stone 3 was $0.8\text{m} \times 0.9\text{m} \times 0.7\text{m}$ and Stone 4 was $0.4\text{m} \times 0.4\text{m} \times 0.4\text{m}$. Stone 3 with cracks was thought to have been broken after hitting the barrier, while the remaining stones seem to be crushed in the movement. The remaining debris has a diameter of about 0.05 m to 0.1 m.



105

Figure 4: Rockfalls piled up in the net.

2.2 Description of the protection project

Two flexible rockfall barriers, Barrier A and Barrier B, have a total length of roughly 140 linear meters and are respectively 70 linear meters long (Fig. 3a). They were situated above the retaining wall at the base of the slope mentioned in Section 2.1.

110 Barrier A, impacted by rockfalls, was the subject of a thorough investigation in this research (Fig. 5a). Eight support posts divided Barriers into seven spans, each 10 meters wide. Two of the seven spans, S1 and S2, were damaged by rockfalls and collapsed. The eight 5 meters high steel columns served as the support posts, numbered P1 – P8, and were bolted to the base with a specific swing space in both the longitudinal and transverse directions (Fig. 5b & 4e). Bolted to the top of the retaining wall were the bases. To guarantee the stability of the steel columns, the upper anchor ropes, border anchor ropes, and guy ropes were snapped to their top (Fig. 5c). The ends of steel columns P1 and P8 were fixed with support ropes (including upper, lower, and border support ropes) by rope buckles (Fig. 5e), the upper support rope of the middle spans was lapped to the top of the support posts (Fig. 5c), and the lower support rope of the middle spans passed through the rings on the column bases (Fig. 5d). As energy-consuming devices, brake rings were used to connect the upper anchor rope, and upper and lower support cables near each column ends (Fig. 5b & 4c). Steel wire rope net and steel wire net made up the interception unit (Fig. 5c).

120 The steel wire net was connected to the steel wire rope net and support ropes by steel wire. Steel wire rope net was woven by winding ropes to the support ropes and hooking to the end of the column. All the steel's anti-rust and corrosion plating remained



125 Component of flexible system for protecting highway slope”.

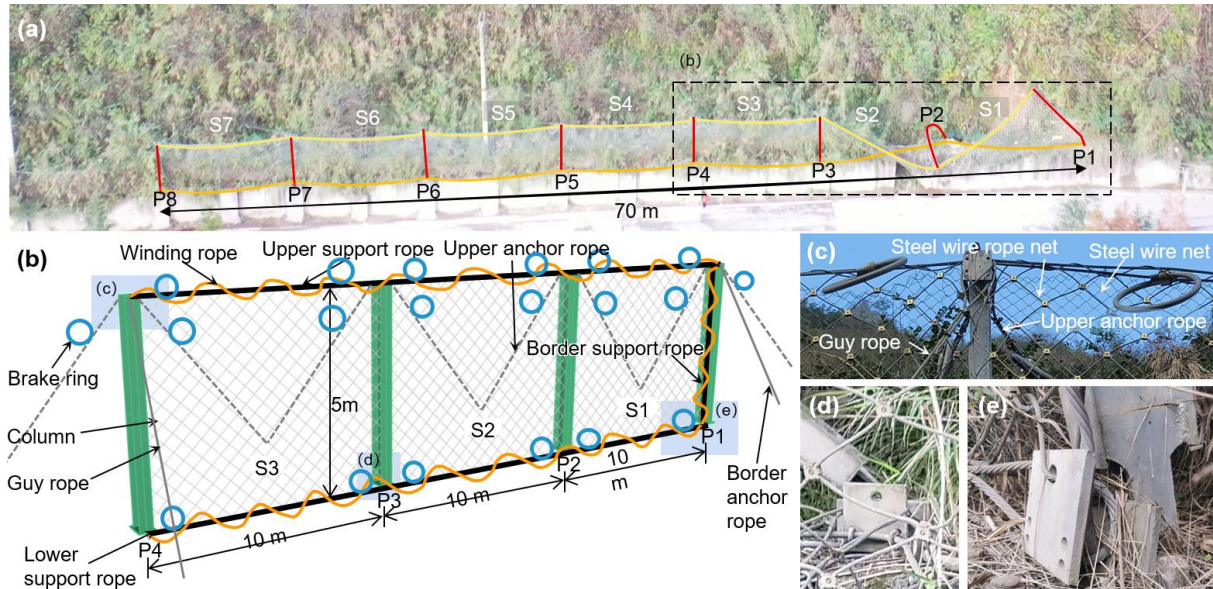


Figure 5: Structure composition of the flexible barrier. (a) Overall photo of the project; (b) Components connection relationship; (c) Column upper end; (d) Base and foot of column in the middle spans; (e) Base and foot of border column.

Table 1: Component specifications of the flexible rockfall barrier project

Support post	Steel column	Height / m	Column distance / m	
	HN200*100	5	10	
Interception unit	Steel wire rope net	Steel wire net		
	CN/08/200/10×5	G/2.2/50		
Steel wire rope	Support rope	Upper anchor rope	Border anchor rope	Winding rope
	2φ12	1φ16	1φ12	1φ8
Energy-consuming devices	Brake ring			
	EDD/40/30/40/R			
Design protection energy	PPS-025 (means 250 kJ, this information is speculative)			

130 *The content of this table adopts the coding structure required by the new specification of the Ministry of Transport of the People’s Republic of China, “JT/T 1328-2020 Flexible protection net system of slope”.

2.3 Damage phenomenon of the flexible rockfall barrier

The flexible rockfall barrier intercepted most of the blocks, but the protection project could not keep offering protection since multiple components broke. The main damage phenomena include:



- 135 (1) Steel column was buckled and destabilized. Due to extreme buckling instability, column P2 could not withstand further pressure (Fig. 6a & 5b).
- (2) Column base was dislodged. The base of steel column P2 detached from the column base on top of the concrete retaining wall (Fig. 6a);
- (3) Rope's anchoring point failed. Due to the anchoring end falling off, the upper anchor ropes connecting steel columns P1 and P2 were not properly functioning (Fig. 6a).
- 140 (4) Steel column was falling. Due to the steel column P1's footing breakdown and the border anchor rope falling off from the column end, the steel column P1 ultimately toppled. Coupled with the instability of steel column P2 and the upper anchor rope breaking off, the interception spans S1 and S2 overturned (Fig. 6a).
- (5) Energy consumption of the brake ring was insufficient. None of the brake rings deployed on this flexible rockfall barrier showed any discernible activity. The brake rings were blocked at the end of the column because them being set on the support ropes in the middle spans. The support ropes were almost impossible to slide (Fig. 6c). The brake rings on the support ropes were directly prevented from being activated by the steel wire rope net and the winding rope since the support ropes were connected to the net by the winding rope (Fig. 6d)
- 145





150 **Figure 6: Damage phenomena of the flexible barrier. (a) The damaged two-span structure; (b) Column P2; (c) Column P3; (d) The connection relationship between the brake ring and the support rope and the steel wire rope net.**

The impact energy of rockfalls on the system is estimated to be minimal because the brake rings lack an evident working phenomenon, the wire rope connecting it is unbroken, and the steel wire rope net is intact.

3 Back analysis of the protection process

155 Numerical simulation has been used to recreate the process of rockfall rolling and impacting the mitigation measure at the investigation site to gain insight into the dynamics process and the causes of protection project damage (Yuen et al., 2023).

3.1 The initial state of the rockfalls impact flexible barrier

The main factors for this back analysis are the impact kinetic energy and impact position of the rocks in contact with the flexible barrier. Using the Rocscience Rocfall2 software, which employs a probabilistic statistical method that integrates slope shape, coefficient of normal restitution (Rn), coefficient of tangential restitution (Rt), friction angle, and roughness, the movement process of the rockfall was simulated to determine the impact energy (Rocscience, 2023; Sun et al., 2019). The slope where the gully was located described in this paper was primarily covered by shrubs, as shown in Fig. 3b, similar to the surface of the slope surface of an engineering site in Songpan, Southwest China, described in Hu et al. (2018). Selected input parameters for the analyses in this study are listed in Table 2. Therefore, as illustrated in Fig. 7a, the slope characteristic parameters employed in this study were in line with those in Hu et al. (2018), and they also fit within the range of the parameters that have been given in (Hu, 1989) for this kind of slope condition. The rockfalls' initial condition parameters of the Rocscience Rocfall analysis were an initial velocity of 0 m/s, a volume of 0.9 m³, and a 2500 kg/m³ density. The crushing of rocks was not considered in this calculation procedure, and the size and source of the stones were constant. There was a total of 10,000 computation cycles

170 **Table 2: Parameters used in RocFall modelling**

Parameters	AB		BC-CD	
	Average	Deviation	Average	Deviation
Rn	0.386	0.04	0.300	0.04
Rt	0.750	0.04	0.800	0.04
Friction angle	22°	2°	20°	2°
Roughness	5°		3°	

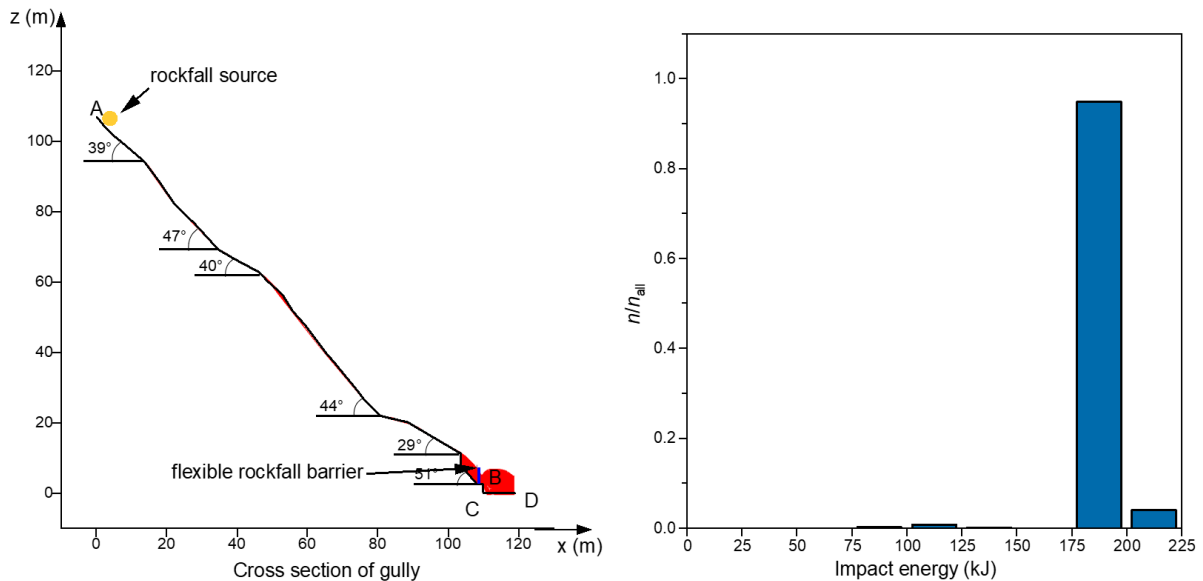


Figure 7: Rockfall movement analysis: (a) Trajectory of rockfall and (b) Probability distribution of kinetic energy of falling rocks at the flexible barrier.

The number of falling rocks that reached the net (n_{all}) after 10,000 calculations was 3433. Fig. 7b depicts the distribution of the kinetic energy of rockfalls that impact the flexible barrier (E_{impact}). E_{impact} ranges from 73.64 kJ to 220.6 kJ, with a maximum value lower than the project's design protection energy level. The final determination of the impact energy of the falling stone on the system was 100kJ in the finite element calculation (Section 3.2), under seven trial calculations with the impact energy were 75, 100, 125, 150, 175, 200, and 225 (unit: kJ). This settled energy is outside the range analyzed to be the most likely, 175kJ to 200kJ. It is assumed that this is because Rocscience Rocfall primarily reflects the macroscopic scenario of rockfall movement on the slope, and less is depicted about the specifics of the rockfall movement process. Fig. 6a indicates that rockfall hit the retaining wall before hitting the passive net; this impact probably considerably reduced the energy of rockfall hitting the flexible barrier.

The lower right-side section of the P2 steel column's lower flange exhibited symptoms of localized damage, leading experts to believe that this was where the collision occurred (Fig. 6a & Fig. 8a). Stone1's starting velocity in Section 3.2 was set to 0.5 m/s, -5 m/s, and 5.5 m/s to ensure it harms the net after hitting the steel column's flange in P2. And for Stones 2, 3, and 4, uniform beginning velocities of -4.8 m/s, -7 m/s, and 4.8 m/s were defined (the velocities listed above are the x, y, and z-axis sub-velocities, shown in Fig. 10).

3.2 Construct the thorough FEM model

The back study of the rockfall impact the flexible rockfall barrier was carried out using the finite element method program ANSYS_2021_R1_LS-DYNA_mpp_r13 (LSTC, 2021). The calculation method is detailed in the literature (Yu et al., 2021, 2018b). The calculation model's components were all constructed of nonlinear materials, and the computational model's



component specifications were similar to the project's. The materials and section types are shown in Table 3. The model is marked as Act_BA.

Table 3: Component specifications of the calculation model

Component	Material	Section
Steel wire rope/ Steel wire rope net	*071_CABLE_DISCRETE_BEAM	* BEAM discrete beam
Brake ring	*S08_SPRING_INELASTIC	* DISCRETE
Steel column	*024_LINEARPLASTICITY_2D (Zhi et al., 2018)	* SHELL
column base	*024_PIECEWISE_LINEAR_PLASTICITY (Zhi et al., 2018)	* SOLID
Rockfall	*020_RIGID	* SOLID

195 Considering this paper focuses on this system's damage mechanism, saving the use of computational resources, and the decay law of impact action between spans (Qi et al., 2014), the FEM model Act_BA was only established for the spans S1, S2, and S3. Support ropes and brake rings were installed on the outside of steel column P3 to ensure a realistic dynamic response on this column (Fig. 8a). Steel column and base material were set with a failure plastic strain of 0.185. The axial force controls the breaking of the wire rope, so the breaking strength of the wire rope with diameters 8mm, 12mm, and 16mm are set to 49.4
 200 kN, 111 kN, and 198 kN, respectively. The steel wire net was not included in the calculation model because it was employed in the project as a member to stop the fine debris and has no noticeable force effect.

Compared to the standard numerical model of flexible rockfall barrier, the following special treatment had been done to reappear the project's actual failure state:

- 205 (1) The column end got a wire rope net attached to it, which caused a small space for the wire rope to slide along. According to multiple trial calculations, the structural deformation was adequate for the best results when the slide amount was set at 0.05 m.
- (2) The winding rope that connects the wire rope net to the support rope is relaxed while the barrier is not in service. However, once the system is impacted, the winding rope of the affected part will elongate, causing the gap between the net and the support rope to expand (Fig. 9a). As a result, extension spring units, which were applied to the connecting unit between the
 210 support rope and the flexible net, were used as equivalent to the winding rope (Fig. 9b). The winding rope spring's ends were fixed. Its constitutive model was bilinear, where k_1 was 1×10^7 N/m, l_1 was 0.1 m, and k_2 was infinite in the model Act_BA (Fig. 9c).
- (3) Due to the phenomena of column foot failure in the actual project (see Section 2.3), the Act_BA model's plastic strain of failure had been defined for the materials at the weld of base connection plates of columns P1 and P2, with values of 0.0065
 215 and 0.007, respectively, after trial calculation.
- (4) After trial calculations, it was determined that the ropes UAR4 and SAR1 would fail at 0.14 seconds and 0.88 seconds after the rockfall contact with the net, respectively.
- (5) Because the UAR2 and UAR3 anchorage points may break before or after impact, a failure tension value of 44900 N was determined after two trial calculations with zero and more than zero failure tension values.



220 The connection damage in Act_BA was corrected, and the same impact condition calculation as in Act_BA—noted as the
control model Ctrl_BA—was carried out to determine the primary source of the damage to this protection structure. The
specific corrective measures are as follows: (1) The anchoring force of the rope’s anchorage point was increased to 396.24kN,
two times the breaking force of an upper anchor rope with a diameter of 16mm. (2) The plastic strain of failure of the materials
at the weld of base connection plates was raised to 0.185. (3) Reinforcing the connection node of column P1 to rope SAR1
225 and the connection node of rope UAR4 to column P2 by setting a failure axial force on the wire rope rather than time control
in Act_BA.

3.3 Simulation results

3.3.1 Protection process

230 The process of rockfall impacting the flexible rockfall barrier is depicted in Fig. 10 as calculated by Act_BA, restoring critical
phenomena like anchor rope shedding, rope anchorage point failure, and base connection plates of column failure. Finally, the
entire protection system was destroyed, and the rockfalls were piled up to the right of the net near the end of column P2,
essentially in the same state as the actual project.

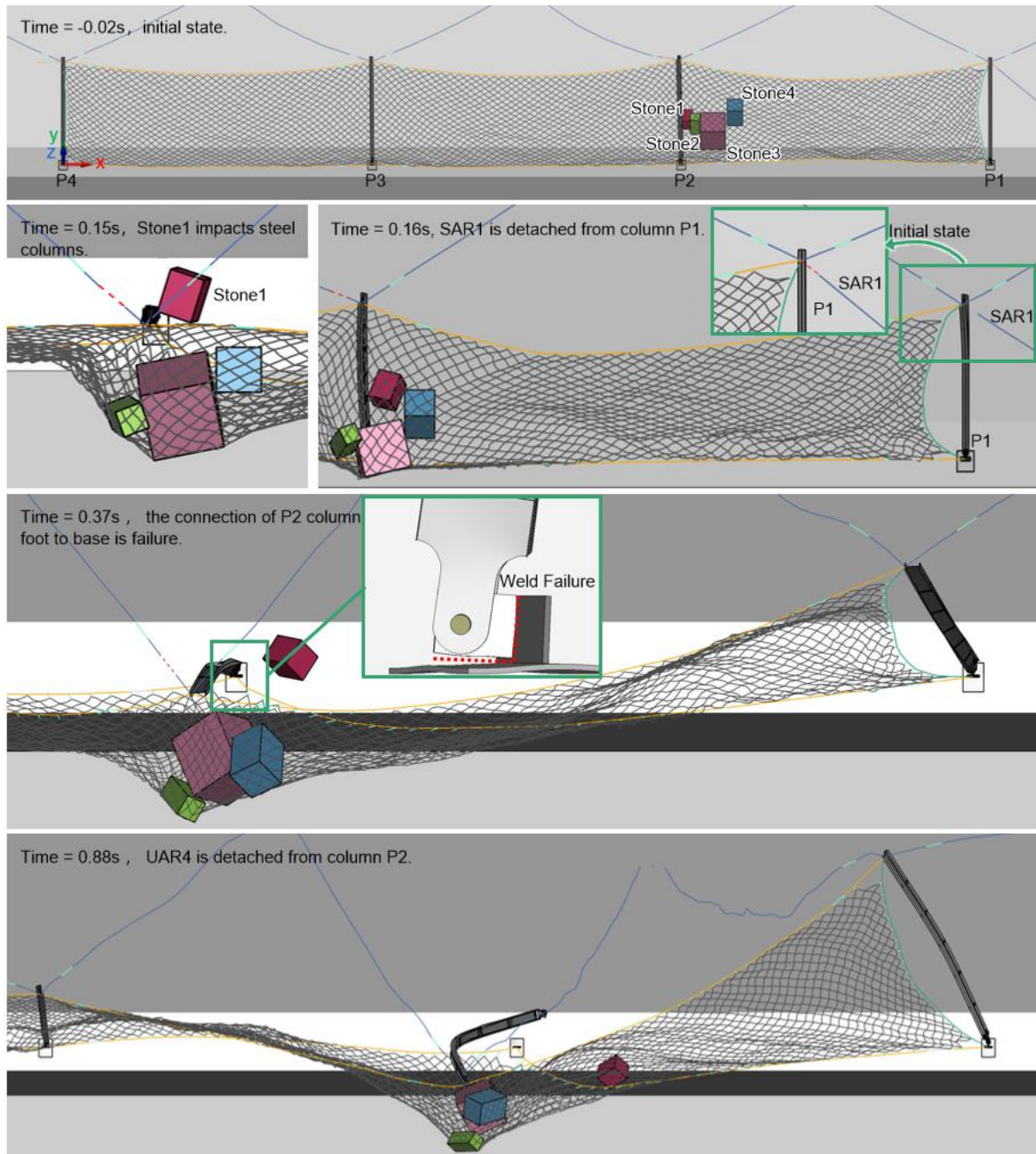
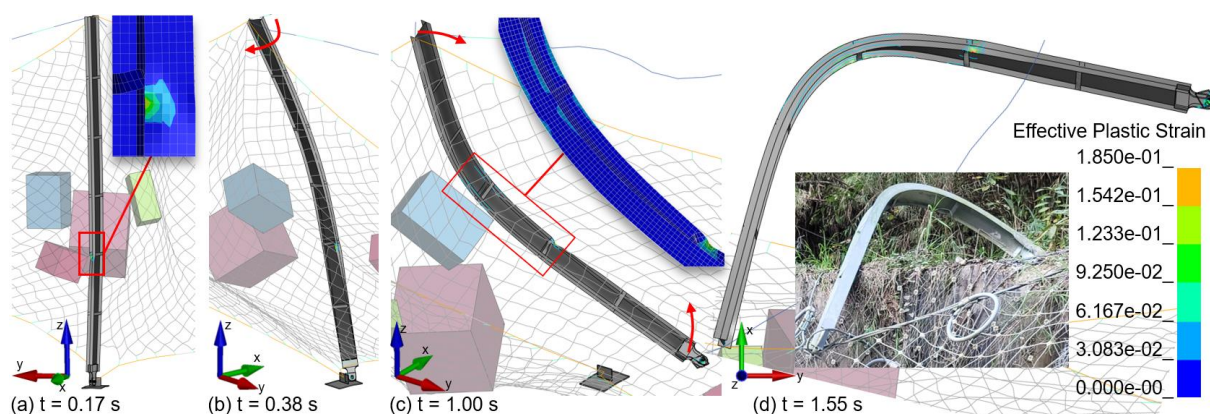


Figure 8: Keyframes of the impact process (the 0 instant occurs when Stone3 touches the wire rope net).



235 3.3.2 Component damage

Like the actual project, the steel column P2 suffered substantial buckling damage, and the flange also sustained localized damage. And border column P1's foot damage caused the column to be dumped entirely. Fig. 11 depicts the buckling progression of steel column P2 in Act_BA: At 0.15 s, Stone1 impacted steel column P2, causing localized damage at the impact point; at 0.25 s, the stress on both sides of the end of the steel column P2 was out of balance after the failure of the anchorage point connected to the ropes UAR2 and UAR3, while the column foot was restrained and the column P2 was twisted; at 0.37 s, the base connection plate of the column P2 welded failed as a result of the column foot twisting, releasing the column P2 from the torsional restraint and turning it into a compression-bending member; at 0.98 s, the column P2 was impacted by the rebounding stone; finally, a C-shaped buckling state was created by constantly compressing and stressing the steel column P2.



245 **Figure 9: Column P2 deformation development in Act_BA.**

The numerical simulation reproduced the phenomena of rope failure, such as the failure of the rope anchorage point connected to upper anchor ropes UAR2 and UAR3 and the disengagement of the side anchor rope SAR1 and upper anchor rope UAR4 from column P1's end. Fig. 12 shows the temporal evolutions of wire ropes' internal force, where all the wire ropes' axial force extreme is below the breaking strength of the corresponding specification wire rope. However, considerable tension pulses were seen in LSR and UAR3 because of the confined member slide deformation. Additionally, each wire rope in the wire rope net had an axial force that was consistently less than the breaking force.

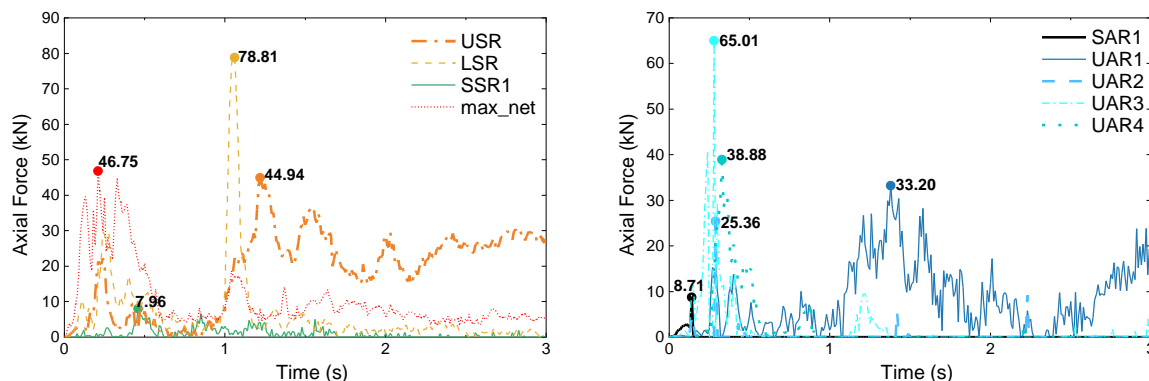


Figure 10: Axial force of the Wire ropes in Act_BA

The simulation result shows that the brake ring connected to the lower support rope near column P1 stretched up to 0.35 meters because the inversion model Act_ did not regulate this elongation. However, in the actual project, the brake ring would be constrained by the wire rope net winding rope and could only stretch up to 0.20 m. There was limited elongation (elongation ≤ 0.02 m) in the other brake rings. Generally, Act_BA's overall impact process and component reaction results aligned with the engineering site's actual situation.

3.3.3 Energy evolution of the protection process

An energy analysis of the protection process was carried out based on the simulation results to assess the protection system's contribution to the interception of rockfalls. The initial moment of impact kinetic energy and falling stone potential energy were taken from the moment the first rock, Stone3, touched the barrier in this paper, even though there were differences in the times at which each rockfall impacts the barrier. The temporal evolution of kinetic energy and potential energy of rockfalls shows that the total impact kinetic energy was 101.4 kJ, which is 40.1% of the design protection energy of the flexible rockfall barrier (Fig. 13). During the protection process, the gravitational potential energy of rockfalls and flexible barrier decreased by 26.5 kJ and by 29.9 kJ, respectively. Therefore, the energy consumed in the protection process (E_{all}) was 157.8 kJ. Table 4 displays the energy distribution during the protection process: The three paths of energy consumption are material elastic-plastic deformation energy consumption, component contact friction energy consumption (including winding rope energy consumption), and system/air damping consumption, with energy consumption of 56.9kJ, 93.9kJ, and 7.0kJ, accounting for 36.06%, 59.51%, and 4.44% of the total energy consumption, respectively. Noteworthy, the steel column consumes 34.7kJ, about 60.83% of the energy consumed by material elastic-plastic deformation.

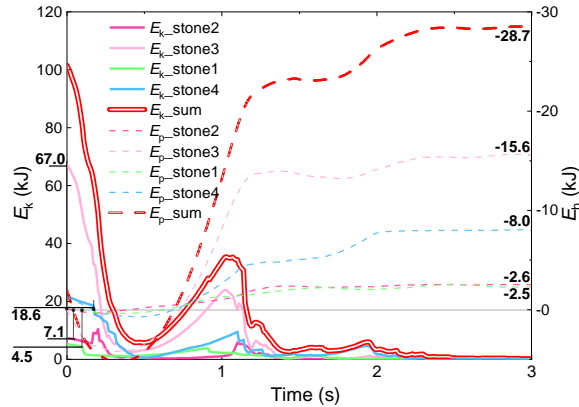


Figure 11: Temporal evolution of kinetic energy and potential energy of rockfalls.

Table 4: Energy consumption statistics of Act_BA.

Path	Position	E (kJ)	E/Eall (%)
material elastic-plastic deformation energy consumption	Brake ring	17.7	11.22
	Steel column	34.6	21.93
	Steel wire rope net/ Steel wire rope	4.6	2.92
Component contact friction energy consumption	Member to member	29.6	18.76
	Stones to barrier	17.4	11.03
	Barrier to retaining wall	24.5	15.53
	Stones to retaining wall	13.4	8.49
	Stone to stone	9.0	5.70
system/air-damping consumption		7.0	4.44

275 3.3.4 Structural damage mechanism

Combining the information from the field investigation and the back analysis, the reasons for the failure of the flexible rockfall barrier are analyzed as follows:

- (1) Unreasonable installation of the flexible net: The wire rope net and the support rope was connected by winding rope; as a result, when the barrier gets impacted, the winding rope would tighten, and the wire rope net could not fully move along the support rope. And the steel column then instantaneously entered the pressure-bending state due to the wire rope net being hooked on the end of the column, which directed the impact force acting on the net to the end of the column.
- (2) Insufficient buffer space for the support rope to the columns: Since the support ropes were fixed to the border column ends, lateral tension would cause the border columns to tilt sideways when the barrier was impacted.
- (3) Unreasonable placement of the brake ring: The brake ring, which should be the component with the highest percentage of energy consumption, only dissipated 17.7 kJ of impact energy, approximately 11.2% of the total energy consumed. This is because the brake ring cannot be fully stretched due to the intertwining of the support rope, winding rope, wire rope net, and brake rings.

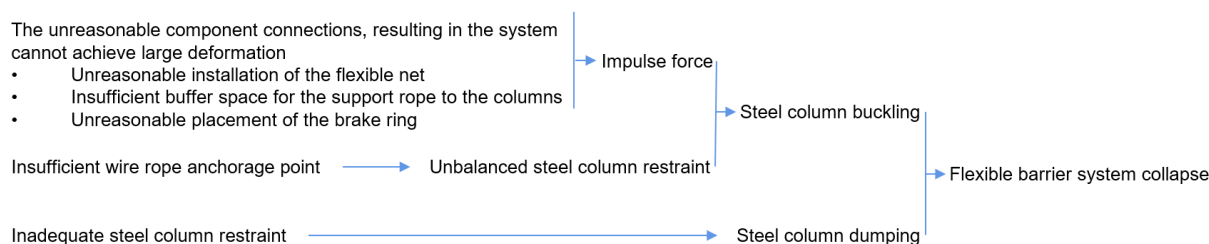


(4) System cannot achieve large deformation: The system deformability was also constrained because the net and support ropes were limited to slide. As a result, the "large deformation" characteristic of flexible barriers was not mirrored in the system, and the impact energy could not be completely dissipated. Additionally, due to the system's limited deformation development, which resulted in a small y-directional pull force transferred from the column end to the upper anchor rope, the brake ring connected to the upper anchor rope could not be fully stretched to release the impact force.

(5) Insufficient wire rope anchorage point: The anchorage points of the upper anchor ropes UAR2 and UAR3 collapsed after the impact due to insufficient anchorage force. Hence UAR2 and UAR3 were unable to stabilize the steel column.

(6) Inadequate steel column restraint: Besides the upper anchor ropes failing as described in (5), the corresponding steel columns lost the essential bond due to the ropes SAR1 and UAR4 falling off from the column ends. Additionally, the steel columns P1 and P2 did not work because the weld failed on the column bases.

Model Ctrl_BA strengthens the connections as well as the wire rope anchorage points. The result of Ctrl_BA shows that column P1 was always in the normal working condition, column P2 did not enter the torsional force state, but column P2 still entered the C-shaped compression bending flexure state as in the Act_BA working condition. Moreover, no damage to the members due to low material configuration was found in the field survey results, model Act_BA or model Ctrl_BA. This means that the three unreasonable connections—unreasonable flexible net installation, insufficient buffer space for the support rope to the columns, and unreasonable placement of the brake ring—are the primary causes of this mitigation project's inability to withstand the rockfall impact. Due to the unreasonable component connection form, a sliding system could not be formed, and the flexible rockfall barrier's buffering mechanism also could not be developed. This resulted in an impulse force at the column end, which eventually caused the steel column to buckle and the system to collapse. Therefore, achieving substantial system deformation requires adequate relative sliding motion between the components, especially the sliding ability of the support rope at the column end (Fig. 14).



310 **Figure 12: Analysis of the system damage mechanism of Act_BA.**

4 Optimization and comparison

4.1 Optimization measures

Whether the support rope allows for sliding at the end of the steel column depends on the connection mechanism employed between the steel column end, the support rope, and the flexible net. The transition rope should be used in most cases where



315 the design protective energy is 1000kJ or less and the support rope does not slide a significant distance along the end of the column (Yu et al., 2018b). The transition rope can prevent the lateral force at the column end and a sharp rise in the axial force of the steel column generated by the net jamming, both of which cause the column to buckle (Fig. 15).

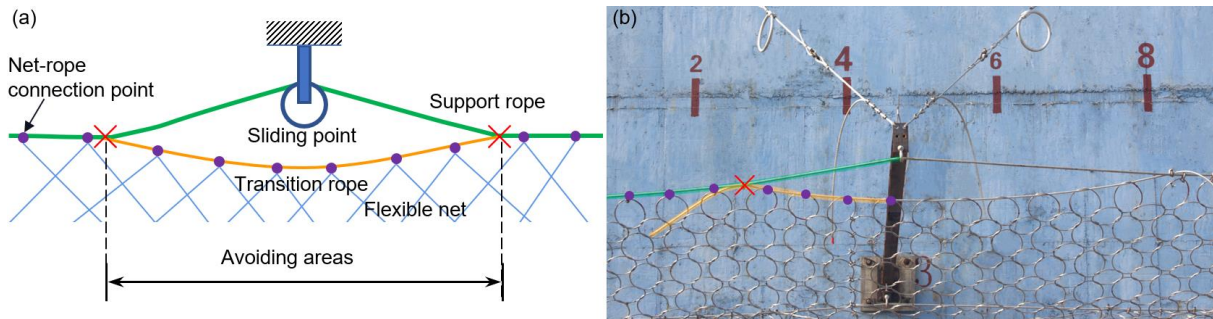
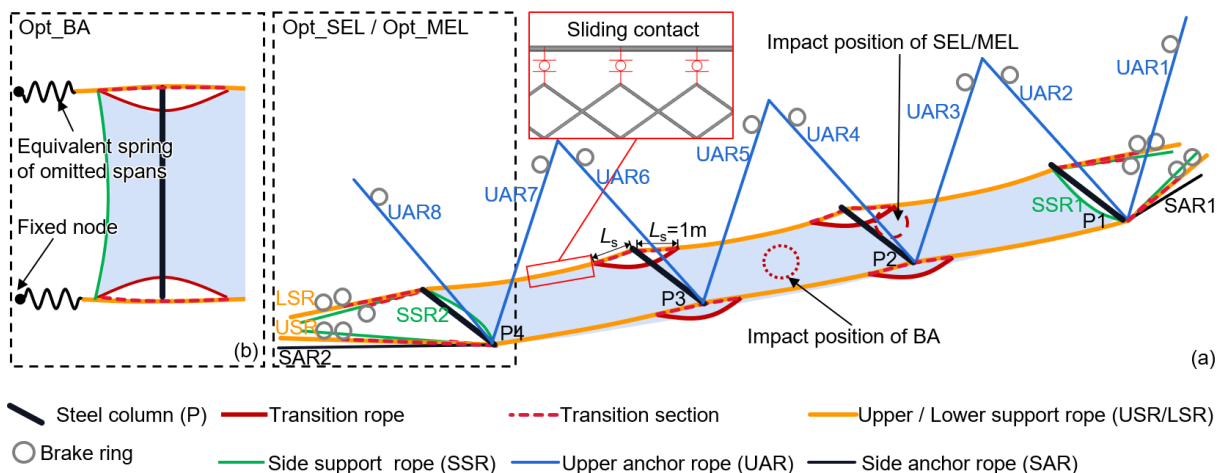


Figure 13: The transition rope applied between column ends and support ropes: (a) Structure schematic and (b) project photo.

320 The control model (Ctrl_) is optimized based on the analysis in Section 3.4, while leaving the specifications of the system components unaltered, and the optimized model is denoted as Opt_ (Fig. 16). The optimization measures are: (1) removing the brake rings from the flexible net connection portion and replacing them with a single brake ring attached to the support rope and all brake rings positioned at the wire rope's anchor end; (2) changing the connection between the column end and the support rope to a transition rope whose length of the transition section L_s set to 1 m, the maximum elongation of the linked
 325 brake ring; (3) extending the support rope from the end of the border column to the slope, and the support rope is in sliding relationship with the border column end; (4) using shackles to link the support ropes to the net or threading the support ropes through the net's holes to ensure that the relative sliding properties between the net and the support ropes; (5) setting an initial x-axis angle of 10° for the barrier to reduce the chance of it being reverse-tipped after impact.



330 **Figure 14: Structure representation of the model Opt_. (a) Simulation models Opt_SEL and Opt_MEL. (b) Simulation model Opt_BA.**



335 Six impact conditions were calculated for the actual model (Act_) and the optimized model (Opt_) of the back-analyst load (BA), service energy level load (SEL), and maximum energy level load (MEL), in addition to the condition calculated as described in Section 3. According to JT/T 1328-2020 / EAD 340059-00-0106, the impactor of SEL and MEL is a single 26-sided block with an impact velocity of 25 m/s, the impact site is the midpoint of the midspan, the MEL impact energy is 250 kJ, and the SEL impact energy is 85 kJ.

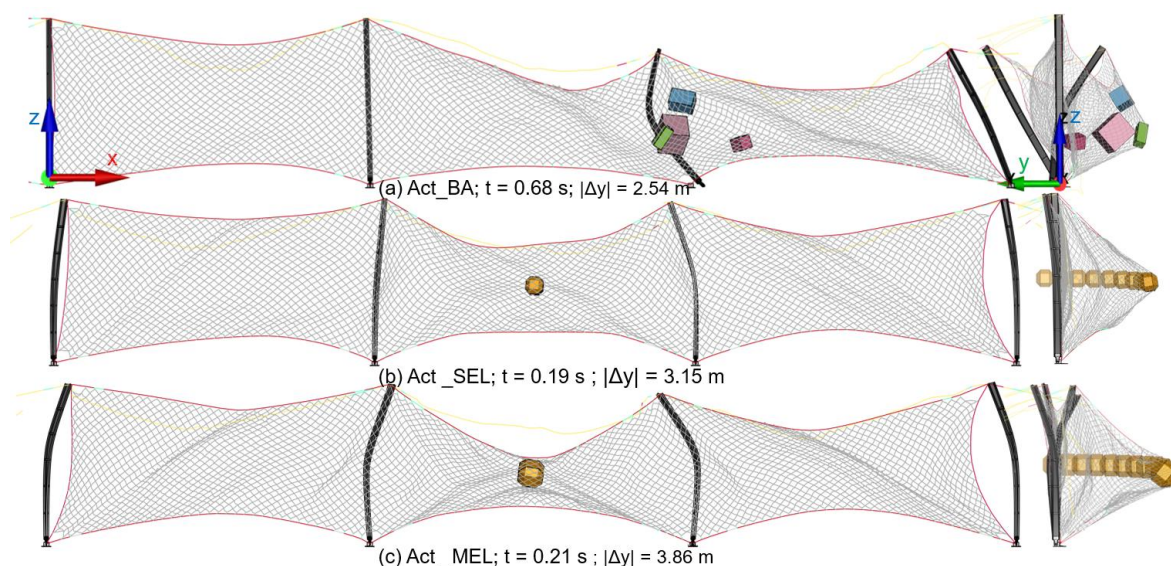
4.2 Results and Comparison

4.2.1 Overall protection up to standard

340 Fig. 17 and Table 5 display the six working conditions' outcomes and structure states. The rockfalls were stopped in all simulation conditions. Still, the model Act_ showed buckling of the steel columns in all impact conditions, significantly weakening the ability of the protection system to continue protecting. If this model had been used for the project, it would have required component replacement and structural repairs before it could continue for protection employment. In the three impact conditions of model Opt_, the entire system maintained structural integrity following impact with no buckling column.

345 In Opt_SEL and Opt_MEL, the barrier successfully intercepted rockfalls, and the barriers were not broken. After completing the interception, the structure of Opt_MEL is described below: as shown in Fig. 17f, the maximum elongation L_{max} is 3.35 meters—the guidelines require L_{max} to be less than 5 meters, and the residual height of the net h_R is 2.85 meters—the guidelines require h_R to be larger than 50% of the nominal height of the kit h_N , which meaning h_R needs to be larger than 2.5 meters. Therefore, the model Opt_ complies with standards for class A flexible rockfall barriers with 250kJ of energy in JT/T

350 1328-2020 and EAD 340059-00-0106.



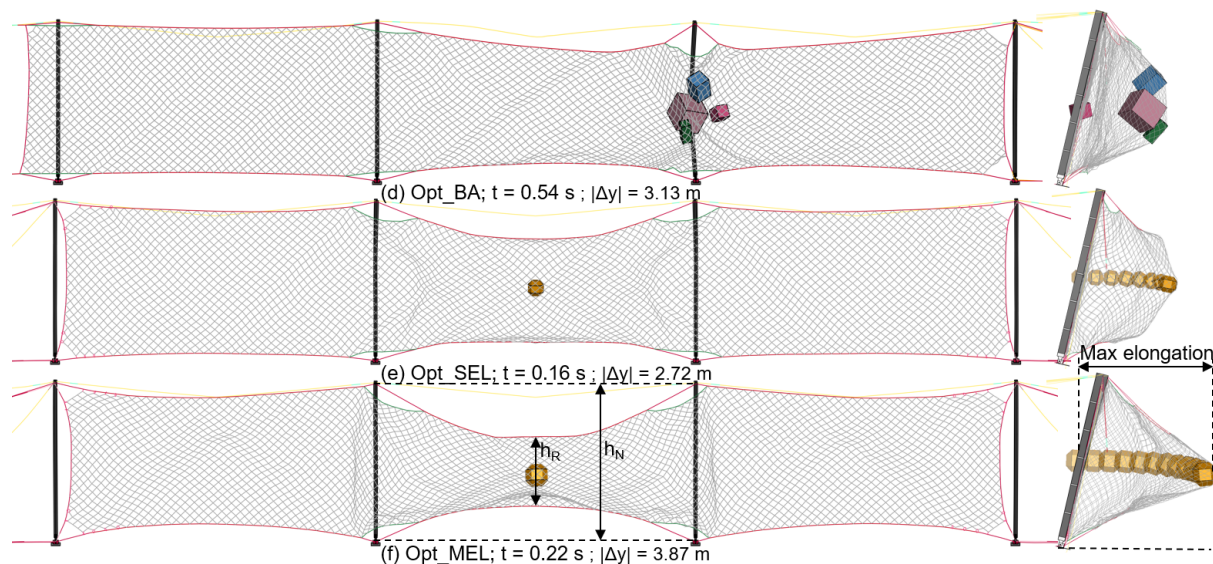


Figure 15: System forms at the moment of maximum y-directional deformation.

Table 5: Description of results for six working conditions.

Working condition	Interception results	Continued protection capability	System final state
Act_BA	Successful interception of rockfall	No	Affected span structure overturning and column P2 bending.
Act_SEL	Successful interception of rockfall	No	Affected span structure overturning and all four columns bending.
Act_MEL	Successful interception of rockfall	No	Affected span structure overturning and all four columns bending.
Opt_BA	Successful interception of rockfall	Yes	Overall structural integrity, steel columns intact.
Opt_SEL	Successful interception of rockfall	Yes	Overall structural integrity, steel columns intact.
Opt_MEL	Successful interception of rockfall	Yes	Overall structural integrity, steel columns intact.

355

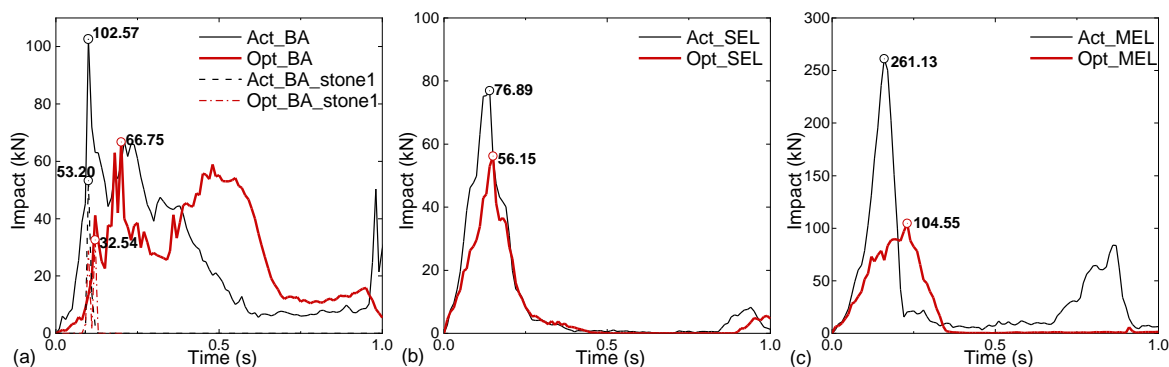
4.2.2 Reduction of structural stress

Compared to the model Act_, the impact force between the rockfalls and the barrier decreased dramatically due to the components' enhanced slidability and the system's improved deformability, which reduced total system stiffness. According to Fig. 18, when model Opt_ is compared to model Act_, the peak impact force falls by 35%, 27%, and 60%, respectively, under the three computational circumstances of BA, SEL, and MEL. It is clear that the protection concept of the flexible protection system "roll with the punches" can be realized effectively and achieve the design protection energy level of the

360



barrier by altering the connection relationships of the column end to the supporting rope and the flexible net to wire rope and the brake ring arrangement position while maintaining the component specifications as-is.



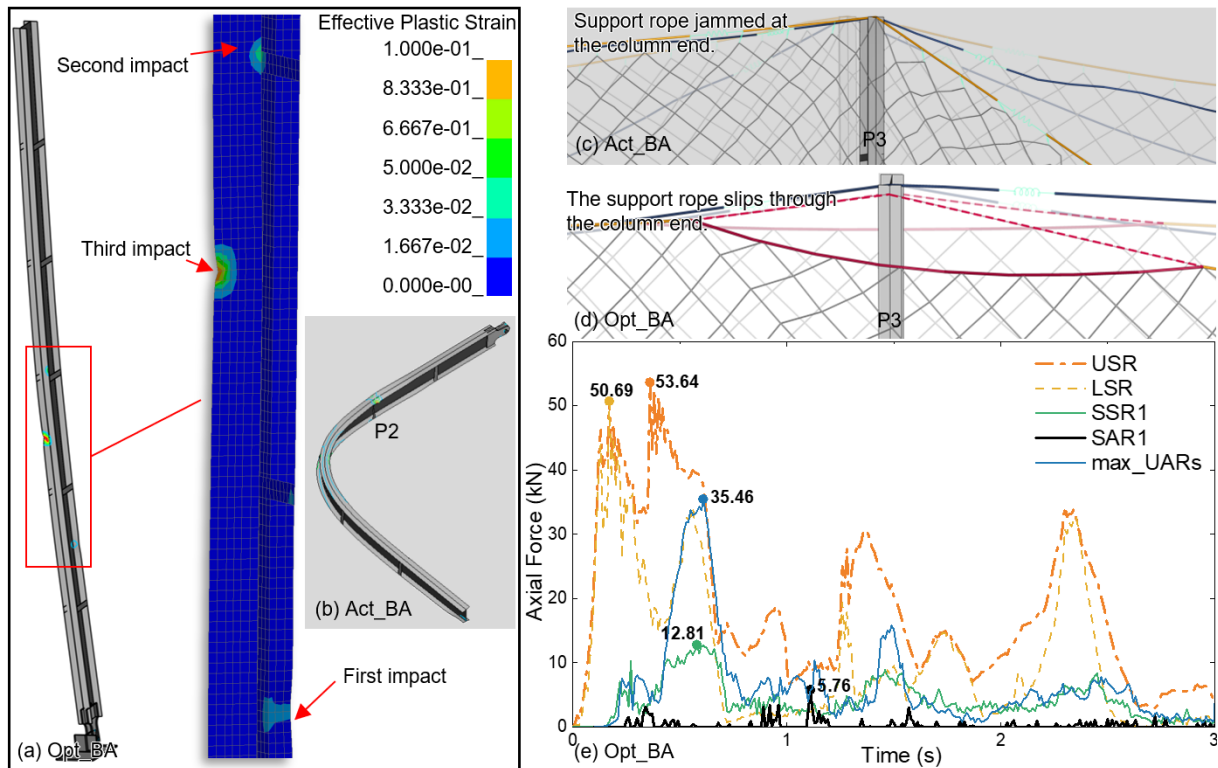
365 **Figure 16: Temporal evolution of the impact of rockfalls and barriers**

Stone1 impacted the steel column P2 in Opt_BA just as it did in the case. Still, due to the different system stiffness, the impact force was almost 39% lower in Opt_BA than it was in Act_BA (Fig. 18a). Although Opt_BA's steel column P2 suffered numerous impacts, none of them seriously damaged it (Fig. 19a). The steel column P2 experienced overall bending at the moment of the most significant system deformation (Fig. 17g). After the impact passed, the steel column recovered, and the entire structure remained stable eventually (Fig. 19a), preventing the system from overthrowing due to the buckling of the steel columns in the Act_BA (Fig. 19b).

370

In Opt_BA, the transition ropes prevented the net from jamming at the column end and lessened the deflection of the column caused by the tugging of the support ropes (Fig. 19c & Fig. 19d). Due to the system's improved deformation capacity, the internal force of the wire rope increased more gradually (Fig. 19e), and the phenomenon of the pulse force of the wire rope as it in Act_BA did not occur (Fig. 12).

375



380 **Figure 17: Opt_BA calculation result: (a) The column P2 in Opt_BA got local damages after several hits. (b) The column P2 in Act_BA was buckling. (c) and (d) are the support rope sliding performance on the end of column P3 in Act_BA and Opt_BA, respectively, where semi-transparent for pre-impact and saturated color for post-impact. (e) The internal force of part of the wire ropes in Opt_BA.**

4.2.3 Energy consumption pathways are optimized

The energy analysis of the Opt_BA protection process was carried out by the method described in 3.3. Simulation. The total impact kinetic energy was 101.4 kJ. During the protection process, the gravitational potential energy of rockfalls and flexible barriers decreased by 28.0 kJ and 7.4 kJ, respectively. Therefore, the actual energy consumed in the protection process of
 385 Opt_BA is 122 kJ. The statistics of energy consumption in Opt_BA are shown in Table 6. The comparison with the results of Act_BA shows the following: In Opt_BA, friction energy dissipation between members replaced elastic-plastic deformation energy dissipation of steel column material as the primary approach for energy dissipation, with an increase in the proportion of this part of energy dissipation from 18.8% (in Act_BA) to 35.2%. Additionally, energy consumed by brake rings, which increased from 11.2% (in Act_BA) to 21.4%, made up the second-largest portion of Opt_BA. The percentage of energy
 390 dissipated by the energy dissipator increased as impact energy increased (In Opt_MEL, the rate of energy consumed by brake rings increased to 33.96% of the total impact kinetic energy consumed in the protection process). In conclusion, after structural optimization, the consumed energy was decreased in "undesirable" paths like buckling energy dissipation of steel columns and



friction energy dissipation between the system and the retaining wall and increased in "desirable" paths like elastic-plastic deformation energy dissipation in energy dissipators and friction energy dissipation in structure components.

395 **Table 6: Energy consumption statistics for Opt_BA and comparison with Act_BA**

Path	Position	Act_BA		Opt_BA		Percentage difference (%)
		E (kJ)	E/Eall (%)	E (kJ)	E/Eall (%)	
material elastic-plastic deformation energy consumption	Brake ring	17.7	11.2	26.1	21.4	10.2
	Steel column	34.7	21.9	7.3	6.0	-15.9
	Steel wire rope net/ Steel wire rope	4.6	2.9	1.1	0.9	-2
Component contact friction energy consumption	Member to member	29.6	18.8	42.9	35.2	16.4
	Stones to barrier	17.4	11.0	17.7	14.5	3.5
	Barrier to retaining wall	24.5	15.5	0.6	0.5	-15
	Stones to retaining wall	13.4	8.5	15.2	12.5	4
	Stone to stone	9.0	5.7	4.4	3.6	-2.1
system/air-damping consumption		7.0	4.4	6.7	5.5	1.1

5 Summary and conclusions

Through the field investigation and the numerical back analysis on a typical flexible rockfall barrier project that is impacted by rockfalls, the phenomenon that the actual impact energy of the flexible barrier is significantly lower than the design protection energy has been studied. The conclusions are as follows:

- 400 1. The system components cannot sufficiently slide between each other, such as the support ropes do not have sufficient slip space at the end of the post, the brake rings are entangled with the flexible net and winding ropes, the flexible net is hooked at the column end, etc., preventing the system from realizing the large deformation of the energy dissipation, and limiting the ability of the brake ring to dissipate energy.
- 405 2. Unreasonable component connections caused the flexible rockfall barrier to break down despite the actual impact energy of the investigated project being only 40.1% of its designed protection energy level. The main damage phenomena of the project include: The steel column being buckled and destabilized, the column footing being dislodged, the rope's anchoring point was failed, the steel column falling, and the energy consumption of the brake ring being insufficient.
- 410 3. Adding transition ropes, anchoring the support ropes to the slope, changing the position of the brake ring of the support ropes from both sides of the column end to the support rope end, and changing the connection between the net and the support rope to a slidable connection can all effectively prevent the instability of the steel columns without modifying the specification of the system's components. The design protection energy and the actual engineering impact condition can both be withstood by the optimized flexible rockfall barrier, and the system's structure is unaffected. Compared with Act_BA, in Opt_BA, the reduction in total system stiffness leads to a reduction in the peak impact force falls by 35%. Furthermore, more impact energy



is consumed by "desirable" paths like elastic-plastic deformation energy dissipation in energy dissipators and friction energy
415 dissipation in structure components.

In conclusion, the disparity between the project conditions and the test conditions is the primary cause of this passive network's
failure in the actual project. For the system to fully utilize the buffering ability of large deformation, the proper assembly
relationship is essential while installing it in the field.

The slope topography, rockfall shape, attack angle, system installation morphology, and other field conditions may influence
420 the performance of the flexible rockfall barrier. The influence of these aspects will be further investigated to provide a
quantitative analysis based on the qualitative in this research. This analysis will serve as a guide for enhancing the dependability
of flexible rockfall barriers.

Acknowledgments

This work has been financially supported by the Sichuan Province Science and Technology Support Program (Grant No.
425 2022YFG0141), the National Key Research and Development Program of China (Grant No.2018YFC1505405), the National
Natural Science Foundation of China (Grant No. 51678504) and the Key Science and Technology Projects in the
Transportation Industry (Grant No. 2020-MS3-101).

Data availability

All raw data can be provided by the corresponding authors upon request.

430 **Author contributions**

Investigation was done by Li-Ru Luo, Zhi-Xiang Yu, Lin-Xu Liao and Li Peng. Data curation was done by Qi Wang. The
statistical analyses were performed by Li-Ru Luo and Li-Jun Zhang. The original manuscript was written by Li-Ru Luo and
Zhi-Xiang Yu. Supervision and funding acquisition were done by Zhi-Xiang Yu.

Competing interests.

435 The authors declare that they have no conflict of interest.

References

Bentley ContextCapture: <https://www.bentley.com/wp-content/uploads/PDS-ContextCapture-LTR-EN-LR.pdf>, last access:
27 July 2023.



- EAD 340059-00-0106: Falling rock protection kits. European Organisation for Technical Approvals, <http://www.eota.eu/>, 27
440 July 2023.
- Ferrero, A. M., Segalini, A., and Umili, G.: Experimental tests for the application of an analytical model for flexible debris
flow barrier design, *Eng. Geol.*, 185, 33–42, <https://doi.org/10.1016/j.enggeo.2014.12.002>, 2015.
- Gentilini, C., Govoni, L., de Miranda, S., Gottardi, G., and Ubertini, F.: Three-dimensional numerical modelling of falling
rock protection barriers, *Comput. Geotech.*, 44, 58–72, <https://doi.org/10.1016/j.compgeo.2012.03.011>, 2012.
- 445 Geobru gg RXE-10000 barrier product profile: [https://www.geobru gg.com/file-78303/downloadcenter/level1-brochures/RXE-
barrier/RXE-10000_product_profile_200131-EN.pdf](https://www.geobru gg.com/file-78303/downloadcenter/level1-brochures/RXE-barrier/RXE-10000_product_profile_200131-EN.pdf), last access: 27 July 2023.
- Hu, H.T. Landslides and rockfalls, China Railway Publishing House, Beijing, China, 183pp., ISBN 9787113004217, 1989. (in
Chinese)
- Hu, J., Li, S.C., Li, L., Shi, S.S., Zhou, Z.Q., Liu, H.L. and He, P.: Field, experimental, and numerical investigation of a rockfall
450 above a tunnel portal in southwestern China, *Bull. Eng. Geol. Env.*, 77, 1365–1382, [https://doi.org/10.1007/s10064-017-
1152-y](https://doi.org/10.1007/s10064-017-1152-y), 2018.
- Jiang, R., Fei, W.P., Zhou, H.W., Huo, M., Zhou, J.W., Wang, J.M., Wu, J.J.: Experimental and numerical study on the load
and deformation mechanism of a flexible net barrier under debris flow impact, *Bull. Eng. Geol. Env.*, 79, 2213–2233,
<https://doi.org/10.1007/s10064-019-01692-y>, 2020.
- 455 J/T 1328-2020, Flexible protection net system of slope. Ministry of Transport of the People’s Republic of China, 2020. (in
Chinese)
- J/T 528-2004, Component of flexible system for protecting highway slope. Ministry of Transport of the People’s Republic
of China, 2004. (in Chinese)
- Kwan, J. S. H., Chan, S. L., Cheuk, J. C. Y., and Koo, R. C. H.: A case study on an open hillside landslide impacting on a
460 flexible rockfall barrier at Jordan Valley, Hong Kong, *Landslides*, 11, 1037–1050, [https://doi.org/10.1007/s10346-013-
0461-x](https://doi.org/10.1007/s10346-013-0461-x), 2014.
- Lei, D.P. and Luo, L.: Research on flexible protection measures and engineering application of high and steep slopes. *Shanxi
Archit.* 20, 58–71. <https://doi.org/10.13719/j.cnki.1009-6825.2021.20.020>, 2021. (in Chinese)
- Liu, C.: Theory and Method of Discrete analysis for Flexible Protective Structure against Geological Hazard on Shallow Slope,
465 Ph.D. thesis, Southwest Jiaotong University, 2020.
- Livermore software technology corporation (LSTC). LS-DYNA keyword user’s manual R13. 2021.
- Luo, L.R., Yu, Z.X., Jin, Y.T., Zhang, L.J., Guo, L.P., Qi, X. and Zhao, S.C.: Quantitative back analysis of in situ tests on
guiding flexible barriers for rockfall protection based on 4D energy dissipation, *Landslides*, 19, 1667–1688,
<https://doi.org/10.1007/s10346-022-01845-3>, 2022.
- 470 Margreth, S. and Roth, A.: Interaction of flexible rockfall barriers with avalanches and snow pressure, *Cold Reg. Sci. Technol.*,
51, 168–177, <https://doi.org/10.1016/j.coldregions.2007.03.008>, 2008.



- Peila, D. and Ronco, C.: Technical Note: Design of rockfall net fences and the new ETAG 027 European guideline, Nat. Hazard. Earth Sys., 9, 1291–1298, <https://doi.org/10.5194/nhess-9-1291-2009>, 2009.
- 475 Qi X., Zhao, S.C., Wei, T., Yu, Z.X., Xu, H.: Test study and numerical analysis of flexible protective structure for falling rocks. Chin. Civ. Eng. J. 47, 62–68. <https://doi.org/10.15951/j.tmgcxb.2014.s2.010>, 2014. (in Chinese)
- Rocscience RocFall software. <https://www.rocscience.com/software/rockfall>, last access: 27 July 2023.
- Rorem, E., Wendeler, C., and Roth, A.: Flexible Debris Flow Barriers in Fire Burned Areas, in: Landslide Science and Practice, edited by: Margottini, C., Canuti, P., and Sassa, K., Springer Berlin Heidelberg, Berlin, Heidelberg, 227–232, https://doi.org/10.1007/978-3-642-31337-0_29, 2013.
- 480 Shi, S. Q., Wang, M., Peng, X. Q., and Yang, Y. K.: A new-type flexible rock-shed under the impact of rock block: initial experimental insights, Nat. Hazard. Earth Sys., 13, 3329–3338, <https://doi.org/10.5194/nhess-13-3329-2013>, 2013.
- Spadari, M., Giacomini, A., Buzzi, O., and Hambleton, J. P.: Prediction of the Bullet Effect for Rockfall Barriers: a Scaling Approach, Rock Mech. Rock Eng., 45, 131–144, <https://doi.org/10.1007/s00603-011-0203-0>, 2012.
- 485 Sun, S.Q., Li, S.C., Li, L.P., Shi, S.S., Wang, J., Hu, J. and Hu, C.: Slope stability analysis and protection measures in bridge and tunnel engineering: a practical case study from Southwestern China, Bull. Eng. Geol. Env., 78, 3305–3321, <https://doi.org/10.1007/s10064-018-1362-y>, 2019.
- Volkwein, A., Schellenberg, K., Labiouse, V., Agliardi, F., Berger, F., Bourrier, F., Dorren, L. K. A., Gerber, W., and Jaboyedoff, M.: Rockfall characterisation and structural protection – a review, Nat. Hazard. Earth Sys., 11, 2617–2651, <https://doi.org/10.5194/nhess-11-2617-2011>, 2011.
- 490 Volkwein, A., Gerber, W., Klette, J. and Spescha, G.: Review of Approval of Flexible Rockfall Protection Systems According to ETAG 027. Geosciences 9, 49. <https://doi.org/10.3390/geosciences9010049>, 2019.
- Wang, M., Shi, S.Q. and Yang, Y.K.: Experimental study of cable anchors for flexible protection systems. Chin. J. Rock Mech. Eng. 32, 2593–2599, 2013. (in Chinese)
- Yang, C., Xia, Q., Wei, H., Yang, P., and Zhu, Y.: Characteristics and Genesis of Dolomites from the Devonian Guanwushan 495 Formation in the Jiguanshan Section, southwest Sichuan Basin, China, <https://doi.org/10.21203/rs.3.rs-2853924/v1>, 2023.
- Yu, Z.X., Qiao, Y.K., Zhao, L., Xu, H., Zhao, S.C. and Liu, Y.P.: A SIMPLE ANALYTICAL METHOD FOR EVALUATION OF FLEXIBLE ROCKFALL BARRIER PART 1: WORKING MECHANISM AND ANALYTICAL SOLUTION, Adv. Steel Constr., <https://doi.org/10.18057/IJASC.2018.14.2.1>, 2018a.
- Yu, Z.X., Qiao, Y., Zhao, L., Xu, H., Zhao, S. and Liu, Y.P.: A SIMPLE ANALYTICAL METHOD FOR EVALUATION 500 OF FLEXIBLE ROCKFALL BARRIER PART 2: APPLICATION AND FULL-SCALE TEST, Adv. Steel Constr., <https://doi.org/10.18057/IJASC.2018.14.2.2>, 2018b.
- Yu, Z.X., Luo, L.R., Liu, C., Guo, L.P., Qi, X. and Zhao, L.: Dynamic response of flexible rockfall barriers with different block shapes, Landslides, 18, 2621–2637, <https://doi.org/10.1007/s10346-021-01658-w>, 2021.



- 505 Yu, Z. X., Zhao, L., Guo, L. P., Liu, Y. P., Yang, C., and Zhao, S. C.: Full-Scale Impact Test and Numerical Simulation of a
New-Type Resilient Rock-Shed Flexible Buffer Structure, *Shock Vib.*, 2019, 1–16,
<https://doi.org/10.1155/2019/7934696>, 2019.
- Yu, Z.X., Zhao, L., Liu, Y.P., Zhao, S.C., Xu, H. and Chan, S.L.: Studies on flexible rockfall barriers for failure modes,
mechanisms and design strategies: a case study of Western China, *Landslides*, 16, 347–362,
<https://doi.org/10.1007/s10346-018-1093-y>, 2019b.
- 510 Yuen, T.Y.P., Weng, M.C., Fu, Y.Y., Lu, G.T., Shiu, W.J., Lu, C.A., Liu, C.Y., Chiu, C.C. and Wen, T.H.: Assessing the
impact of rockfall on a bridge by using hybrid DEM/FEM analysis: A case study in Central Taiwan, *Eng. Geol.*, 314,
107000, <https://doi.org/10.1016/j.enggeo.2023.107000>, 2023.
- Zhao, S.C., Yu, Z.X., Zhao, L., Qi, X. and Wei, T.: Damage mechanism of rockfall barriers under strong impact loading. *Eng.
Mech.* 33, 24–34. <https://doi.org/10.6052/j.issn.1000-4750.2016.06.ST08>, 2016. (in Chinese)
- 515 Zhi, X.D., Zhang, R., Lin, L. and Fan, F. Dynamic constitutive model of Q235B steel and its application in LS-DYNA. *Explos.
Shock Waves*. 38, 596–602. DOI: 10.11883/bzycj-2016-0286, 2018. (in Chinese)